Hindawi
Complexity
Volume 2020, Article ID 8854472, 12 pages
https://doi.org/10.1155/2020/8854472

Research Article

Multiphase SVPWM Strategy Analysis and Implementation of Seven-Phase Permanent Magnet Synchronous Motor

Mingli Lu,[1] **Dong Zhang**,[1] **Benlian Xu**,[2] **Haodong Yang**,[1] **and Yi Xin**[2]

[1]*School of Electrical & Automatic Engineering, Changshu Institute of Technology, Changshu 215500, China*
[2]*School of Mechanical Engineering, Changshu Institute of Technology, Changshu 215500, China*

Correspondence should be addressed to Benlian Xu; xu_benlian@cslg.edu.cn

Received 19 August 2020; Revised 19 September 2020; Accepted 8 October 2020; Published 21 October 2020

Academic Editor: Rui Wang

The multiphase motor drive systems have become a focus in many application areas such as ship electric propulsion, urban mass transit, aerospace, and weapon equipment, as they are characterized by high power density, low torque pulsation as small torque ripple, large output power, strong fault tolerance, and high reliability. However, with the increase of the phase number of the motor, the current harmonic component increases correspondingly, which leads to the decrease of the control performance compared with the three-phase system. In order to overcome this challenge, implementation method of driving control technology for seven-phase permanent magnet synchronous motor (PMSM) based on SVPWM algorithm is discussed thoroughly in this paper. Simulink and experiments have been developed to check its practical feasibility. The results show that the near-six vector SVPWM algorithm (NSV-SVPWM) achieves better performance than other methods.

1. Introduction

Multiphase PMSM is widely used in special occasions such as high current and high voltage, and it works in the case of low voltage and high power drive without any restriction of current or voltage. Compared with three-phase permanent magnet motor, PMSM has many advantages, such as simple structure, small volume, high power output density, high efficiency, low torque ripple, and low vibration noise, and it has been widely used in the field of micro electric vehicle [1–5]. As the number of motor phases increases, the pulse frequency of the output torque of the multiphase motor drive system increases, and the amplitude of the mechanical torque ripple decreases; thus, the static and dynamic performance of the multiphase motor drive system can be improved, and the reliability of the whole drive system is improved. For the dimension of the multiphase motor drive system, the three-dimensional system of the traditional three-phase motor is transformed into a multidimensional system. The increase of the dimension of the motor makes the control strategy of the multiphase motor more abundant, thus making the more complex motor control algorithm more easily realized.

In view of the above advantages of multiphase PMSM, the seven-phase PMSM is considered. However, due to the increase of the phases of motors, the current harmonic contents of multiphase motor system are larger, which leads to the decrease of the control performance compared with the three-phase system [6, 7]. The inverter nonlinearity is the key source of current harmonics. To solve this problem, domestic and foreign experts and scholars have conducted a lot of research [6, 8–10], such as starting from the design improvement of motor, changing the distribution of motor winding and distribution of groove to reduce the harmonic current, and starting from the angle of control strategy, current decoupling to different harmonic subspaces to reduce the harmonic content [6].

With regard to the PWM of seven-phase system, the SVPWM theory can be still employed to represent the behavior of seven-phase systems as a natural extension of the traditional three-phase SVPWM transformation [11, 12]. In this paper, the space vector modulation (SVM) has been extended to a seven-phase voltage source inverter, considering reference space vectors in all the three d-q planes [13]. Especially, the proposed SVM strategy univocally selects the

inverter switch configurations among the 128 possibility by privileging the space vector on the first subspace plane, $d1$-$q1$, the one responsible of balanced sinusoidal output voltage waveforms [14]. Then, vector analysis of the other two planes that produce the harmonic current is made to find out whether the vector that generates harmonics can be counteracted as much as possible. So, the implementation method of driving control algorithm based on SVPWM for low-order current harmonics suppression is discussed in this paper.

The goal of this paper is design a framework that addresses the above challenges. First, the mathematical model of the static coordinate system of the seven-phase PMSM is analyzed in detail. Then, a novel synchronous rotating coordinate transformation matrix was presented, and a mathematical model of the rotating coordinate system is obtained by matrix converter. And then, the 3rd harmonic subspace and the 5th harmonic subspace are derived based on the spatial voltage vector distribution of seven-phase bridge inverter. After analyzing the performance of these methods, namely, the near-four vectors SVPWM (NFV-SVPWM) algorithm and NSV-SVPWM algorithm, NSV-SVPWM algorithm is carried out. Finally, a driving control platform based on STM32F407 primary control chip is designed for seven-phase PMSM.

Preliminary results have been announced in the conference paper [15]. A more complete framework of control technology of seven-phase PMSM for low-order current harmonics suppression is proposed. We also describe in detail the experiments analysis. The rest of the paper is organized as follows. Section 2 gives mathematic model of seven-phase PMSM. The seven-phase SVPWM algorithm is described in Section 3. Simulations and experiments analysis of PMSM and the detailed discussion are described in Section 4. Finally, a summary is provided in Section 5.

2. Mathematic Model of Seven-Phase PMSM

The investigated motor is a hidden pole type seven-phase PMSM. Before studying the driving control system of the seven-phase PMSM, the mathematical model of the motor is established at first. Therefore, for the convenience of analysis, the following assumptions are made for the seven-phase PMSM studied:

(1) Neglect the influence of eddy current and hysteresis in iron core

(2) The magnetic circuit of the motor is linear, and the saturation effect will not occur

(3) The stator surface of the motor is smooth

(4) Neglect influence of motor temperature on motor winding

(5) The structure of the motor is implicit, and the reactance is equal

(6) The seven-phase winding is "Y" type connection, and the spatial distribution is completely symmetrical

In the stationary coordinate system, the flux equation, the stator voltage equation, the electromagnetic torque equation, and the mechanical motion equation are important mathematical model of the seven-phase PMSM.

In natural coordinate, the voltage equation for seven-phase PMSM is given:

$$U_v = R_v I_v + g\psi_v, \tag{1}$$

where $U_v = \left[u_a,\ u_b,\ u_c,\ u_d,\ u_e,\ u_f,\ u_d \right]^T$ is the stator voltage matrix, R_v represents the stator resistance matrix, $I_v = \left[i_a,\ i_b,\ i_c,\ i_d,\ i_e,\ i_f,\ i_d \right]^T$ is denoted as the stator current matrix, and $g = \mathrm{d}/\mathrm{d}t$. $\psi_v = \left[\psi_1,\ \psi_2,\ \psi_3,\ \psi_4,\ \psi_5,\ \psi_6,\ \psi_7 \right]^T$ is interpreted as the stator flux matrix.

The flux equation for seven-phase PMSM is given:

$$\psi_v = L_v I_v + \psi_n, \tag{2}$$

where L_v is the stator inductance matrix, and Ψ_n represents the flux linkage of permanent magnet. It can be defined as

$$\psi_n = \psi \begin{bmatrix} \cos\theta \\ \cos(\theta - \alpha) \\ \cos(\theta - 2\alpha) \\ \cos(\theta - 3\alpha) \\ \cos(\theta - 4\alpha) \\ \cos(\theta - 5\alpha) \\ \cos(\theta - 6\alpha) \end{bmatrix}, \tag{3}$$

where ψ, θ are the flux linkage amplitude of permanent magnet and the rotor position angle, respectively. $\alpha = 2\pi/7$ is the angle between adjacent two-phase winding axes.

The torque equation for seven-phase PMSM is given:

$$\begin{cases} \mathrm{M}_{\mathrm{eo}} = \dfrac{1}{2} I_v^T L_v I_s + I_v^T \psi_n, \\ \\ T_{\mathrm{e}} = a \dfrac{\mathrm{dM}_{\mathrm{eo}}}{\mathrm{d}\theta}, \end{cases} \tag{4}$$

where T_{e} is motor electromagnetic torque, M_{eo} is denoted as motor magnetic energy, and a is the polar logarithm of motor.

For the hidden pole rotor of motor, L_v and θ are independent of each other, then the above function can be rewritten as

$$T_{\mathrm{e}} = a \frac{\mathrm{dM}_{\mathrm{eo}}}{\mathrm{d}\theta} = a \left[I_v \frac{\mathrm{d}\psi_n}{\mathrm{d}\theta} \right]. \tag{5}$$

The mechanical motion equation for seven-phase PMSM is

$$\frac{J}{a} \frac{\mathrm{d}\omega_r}{\mathrm{d}t} = T_{\mathrm{e}} - T_{\mathrm{l}}, \tag{6}$$

where T_l is denoted as motor load torque, and J is moment of inertia of mechanical and electrical system. Seven-phase

PMSM is a nonlinear system. The methods [16, 17] can provide a reference for some parameters estimated and model constructed.

According to equations (2)–(6) of electromagnetic torque equation, it can be seen that the straight axis and quadrature axis currents of stator of seven-phase PSMS are coupled with each other, which brings inconvenience to the subsequent research on vector control theory. Therefore, it is necessary to select appropriate spatial transformation and simplify the mathematical model of the seven-phase PMSM.

According to the principle of constant power, the transformation matrix from natural coordinate system to rotating coordinate system $(d_1 - q_1 - d_3 - q_3 - d_5 - q_5 - 0)$ based on the matrix transformation of Clark and Park is given by

$$\Pi(\theta) = \sqrt{\frac{2}{7}} \begin{bmatrix} \cos\theta & \cos(\theta-\alpha) & \dots & \cos(\theta+\alpha) \\ -\sin\theta & -\sin(\theta-\alpha) & \dots & -\sin(\theta+\alpha) \\ \cos 3\theta & \cos 3(\theta-\alpha) & \dots & \cos 3(\theta+\alpha) \\ -\sin 3\theta & -\sin 3(\theta-\alpha) & \dots & -\sin 3(\theta+\alpha) \\ \cos 5\theta & \cos 5(\theta-\alpha) & \dots & \cos 5(\theta+\alpha) \\ -\sin 5\theta & -\sin 5(\theta-\alpha) & \dots & -\sin 5(\theta+\alpha) \\ 1 & 1 & \dots & 1 \end{bmatrix}. \tag{7}$$

If equation (7) is introduced into equations (2)–(6), through matrix transformation, the mathematical model of the motor in the rotating coordinate system can be obtained.

The voltage equation for seven-phase PMSM is given by

$$\begin{aligned} U_{\mathrm{dq}} &= \Pi(\theta)U_v = \Pi(\theta)R_v I_v + \Pi(\theta)g\Psi_v \\ &= \Pi(\theta)R_v\Pi(\theta)^{-1}\Pi(\theta)I_v + g\left[\Pi(\theta)\Psi_v\right] - g\Pi(\theta)\Pi(\theta)^{-1}\Pi(\theta)\Psi_v \\ &= R_{\mathrm{dq}}I_{\mathrm{dq}} + g\Psi_{\mathrm{dq}} + \Lambda\Psi_{\mathrm{dq}}, \end{aligned} \tag{8}$$

where $U_{\mathrm{dq}} = \Pi(\theta)U_v = \left[\, U_{d1} \;\; U_{q1} \;\; U_{d3} \;\; U_{q1} \;\; U_{d1} \;\; U_{q3} \;\; 0 \,\right]^T$

$$\begin{aligned} R_{\mathrm{dq}} &= \Pi(\theta)R_v\Pi(\theta)^{-1} = r_v I_{7\times 7}, \\ I_{\mathrm{dq}} &= \Pi(\theta)I_v = \left[\, i_{d1} \;\; i_{q1} \;\; i_{d3} \;\; i_{q1} \;\; i_{d1} \;\; i_{q3} \;\; 0 \,\right]^T, \\ \Psi_{\mathrm{dq}} &= \Pi(\theta)\Psi_v = \left[\, \Psi_{d1} \;\; \Psi_{q1} \;\; \Psi_{d3} \;\; \Psi_{q1} \;\; \Psi_{d1} \;\; \Psi_{q3} \;\; 0 \,\right]^T. \end{aligned} \tag{9}$$

In this way, other equations can be obtained. The flux equation for seven-phase PMSM is given by

$$\Psi_{\mathrm{dq}} = \Pi(\theta)\Psi_v = \Pi(\theta)\left(L_v I_v + \Psi_n\right). \tag{10}$$

For the hidden pole rotor of motor, the torque equation can be calculated as

$$\begin{aligned} T_{\mathrm{e}} &= \frac{\partial \mathrm{M}_{\mathrm{eo}}}{\partial\theta} = a\left[I_v\frac{\partial\Psi_n}{\partial\theta}\right] \\ &= \frac{7}{2}aI_{\mathrm{dq}}^T\Pi(\theta)\frac{\partial\Psi_n}{\partial\theta} \\ &= \frac{7}{2}\alpha\Psi i_{q1}, \end{aligned} \tag{11}$$

where i_{q1} is the component of stator current on the q axis.

3. Seven-Phase SVPWM Algorithm

3.1. Seven-Phase Bridge Inverter. The seven-phase motor drive systems are generally supplied by a seven-phase voltage source bridge inverter. Similar to three-phase bridge inverter, the topology of seven-phase bridge inverter is connected by 14 power switch devices, as shown in Figure 1.

In order to approach the circular magnetic field well, there should be as many regular polygon edges as possible; that is, more inverter switching state combinations should be generated. For seven-phase voltage inverter, the state variable S_i $(i = a, b, c, d, e, f, g)$ is introduced to represent the switching state of each bridge arm, and the turn-off and turn-on of the switch are represented by "0" and "1." Then, the seven-phase voltage type inverter can be combined into $27 = 128$ switching states [18, 19].

In a multiphase voltage source inverter (VSI), switching states determine load equivalent circuit configurations. Therefore, switching states can be divided into corresponding sets. In a seven-phase inverter, these basic equivalent circuit configurations can be categorized into three types, namely, $C16$ equivalent circuit, $C25$ equivalent circuit, and $C34$ equivalent circuit, as shown in Figure 2. Therefore, the switching states can be represented by three sets: $\{C16\}$, $\{C25\}$ and $\{C34\}$.

From the above, the space vector is obtained as

$$\begin{cases} U_{v1} = \dfrac{2}{7}U_{\mathrm{dc}}\left(S_a + \alpha S_b + \alpha^2 S_c + \alpha^3 S_d + \alpha^4 S_e + \alpha^5 S_f + \alpha^6 S_g\right), \\ U_{v3} = \dfrac{2}{7}U_{\mathrm{dc}}\left(S_a + \alpha^3 S_b + \alpha^6 S_c + \alpha^2 S_d + \alpha^5 S_e + \alpha S_f + \alpha^4 S_g\right), \\ U_{v5} = \dfrac{2}{7}U_{\mathrm{dc}}\left(S_a + \alpha^5 S_b + \alpha^3 S_c + \alpha S_d + \alpha^6 S_e + \alpha^4 S_f + \alpha^2 S_g\right). \end{cases} \tag{12}$$

Aiming to produce the desired fundamental (sinusoidal) component in the output phase voltage without low-order harmonics, SVPWM algorithm is used. Supposing that the DC bus voltage is considered as "1," Table 1 presents the magnitude relation of the voltage vector.

3.2. Current Harmonics Suppression Method. Current harmonics (3rd, 5th) caused by the inverter nonlinearity in phase currents are considered. To increase efficiency and

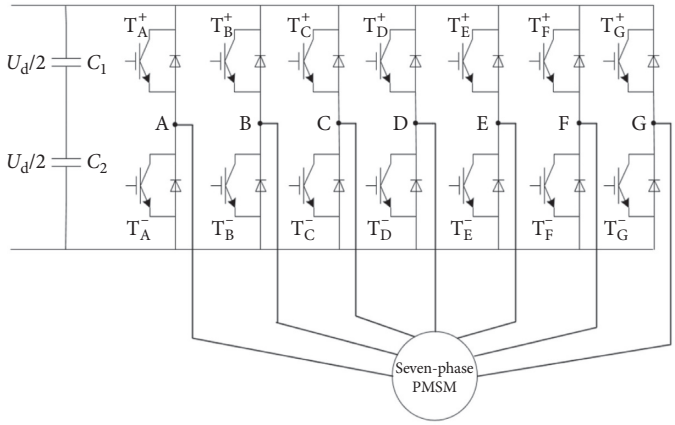

Figure 1: Main circuit of seven-phase bridge inverter.

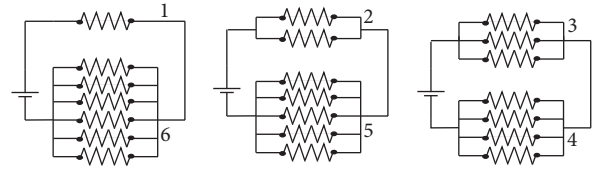

Figure 2: Switch combination equivalent circuit.

Table 1: Voltage vector amplitude relation table.

Vectors	U_a	U_b	U_c	U_d	U_e	U_f	U_g
Amplitude	$0.127U_{dc}$	$0.159U_{dc}$	$0.229U_{dc}$	$0.286U_{dc}$	$0.356U_{dc}$	$0.515U_{dc}$	$0.642U_{dc}$

performance of multiphase power converters, the current total harmonic should be eliminated, which highly relies on their control strategy. In this section, two control strategies of SVPWM algorithm are presented in detail.

3.2.1. The NFV-SVPWM Algorithm. Through analysis of the near-four vectors SVPWM (NTV-SVPWM) algorithm [15], it is found that the medium and small vector groups of the space voltage vector in the seven-phase motor system are not fully utilized to remove the harmonic component of the phase current. Therefore, we take into account the more abundant basic voltage vectors in the seven-phase inverter to reduce the harmonic component. Two near vectors, two large vectors, and zero vectors in the fundamental wave subspace are used to synthesize the reference voltage vector, that is, NFV-SVPWM algorithm [20], whose control strategy is the same as the three-phase SVPWM. The reference voltage in the sector is obtained by using the parallelogram rule synthesis. The maximum voltage vector and the middle vector correspond to the U_g vector group and the U_f vector group in Table 1, respectively.

The NFV-SVPWM algorithm of seven-phase motor system follows the following principles: The selected basic voltage vectors are given the voltage reference vector in the synthetic fundamental wave space, and the voltage vector synthesized in the 3rd harmonic subspace should be guaranteed to be zero. As shown in Figure 3, in the basic wave space, voltage vectors U_{71}, U_3 and U_{67}, U_{103} are in the same direction, while in the 3rd harmonic subspace, voltage vectors U_{71}, U_3 and U_{67}, U_{103} are opposite to each other in direction. In order to make the voltage vector of the 3rd harmonic subspace zero, the action time of voltage vectors U_{71}, U_3 and U_{67}, U_{103} is inversely proportional to the amplitude of the voltage vector in the 3rd harmonic subspace. In this way, the voltage vectors cancel each other without affecting the synthesis of voltage vectors in fundamental wave space.

For example, in the first sector, fundamental voltage vectors $U_3, U_{67}, U_{71}, U_{103}$ and U_0, U_{127} two zero vectors are

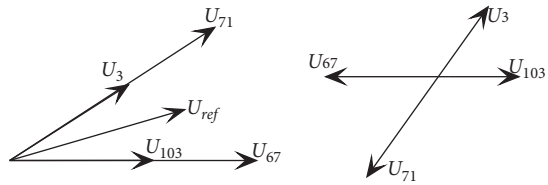

Figure 3: NFV-SVPWM vector synthesis. (a) Fundamental wave subspace. (b) The 3rd harmonic subspace.

selected to synthesize the reference vector U_{ref}. The time of action is defined as T_1, T_2, T_3, T_4 and T_0, respectively.

Similar to the NTV-SVPWM analysis method, the following relations can be obtained:

$$\begin{cases} T_1 = \dfrac{U_\alpha \sin[(m-1)(\pi/7)] - U_\beta \cos[(m-1)(\pi/7)]}{\left(1+1.2466^2\right)\left|U_M\right|\{\cos(m\pi/7)\sin[(m-1)(\pi/7)] - \sin(m(\pi/7))\cos[(m-1)(\pi/7)]\}} T_s, \\ T_2 = 1.2466 T_4, \\ T_3 = 1.2466 T_1, \\ T_4 = \dfrac{U_\alpha \sin(m(\pi/7)) - U_\beta \cos(m(\pi/7))}{\left(1+1.2466^2\right)\left|U_M\right|\{\cos(m(\pi/7))\sin[(m-1)(\pi/7)] - \sin(m(\pi/7))\cos[(m-1)(\pi/7)]\}} T_S. \end{cases} \tag{13}$$

To reduce the switching losses, the switching signal of the voltage vector in sector one is shown in Figure 4.

3.2.2. The NSV-SVPWM Algorithm. It is well known that 6 groups of voltage vector can synthesize the desired voltage vector. However, voltage vectors U_a, U_b, U_c and U_e with small amplitude are not continuously switched, which lead to desired voltage vector different direction. So, the voltage vector of the stator flux may offset. In NSV-SVPWM algorithm, the reference vector needs six voltage vectors to be synthesized in each sector of the fundamental wavelet subspace. The previous analysis shows that only three vectors U_d, U_f, and U_g of seven groups of voltage vectors in the fundamental subspace are used. Therefore, NSV-SVPWM algorithm is used to synthesize the reference voltage vector by a total of three groups of six voltage vectors: U_d, U_f, and U_g.

For example, in the first sector, select fundamental voltage vectors U_1, U_3, U_{67}, U_{71}, U_{103}, U_{111} and two zero vectors U_0, U_{127} to synthesize the reference vector U_{ref}. The time of action is defined as T_1, T_2 T_3, T_4, T_5, T_6 and T_0, respectively.

Aiming to cut down the harmonic content of phase current, the voltage vector synthesized in the $\alpha_3 - \beta_3$ and $\alpha_5 - \beta_5$ subspaces should be zero. As shown in Figure 5, it can be seen that voltage vectors U_1, U_{67} and U_{103} are in the same direction in $\alpha_1 - \beta_1$ subspace, while vector U_{67} is opposite to the corresponding two vectors in the $\alpha_3 - \beta_3$ and $\alpha_5 - \beta_5$ subspaces. To make the synthesized voltage vectors be zero in the subspaces $\alpha_3 - \beta_3$ and $\alpha_5 - \beta_5$, the reverse vector can be counteracted by the corresponding two other vectors. Thus, the resultant voltage of each direction is zero, and the current harmonic is suppressed.

In the $\alpha_1 - \beta_1$ fundamental subspace, the following equations came up

$$\begin{cases} U_{\alpha 1} = \dfrac{T_1}{T_s}\left|U_1\right| + \dfrac{T_2}{T_s}\left|U_3\right|\cos\dfrac{\pi}{7} + \dfrac{T_3}{T_s}\left|U_{67}\right| + \dfrac{T_4}{T_s}\left|U_{71}\right|\cos\dfrac{\pi}{7} + \dfrac{T_5}{T_s}\left|U_{103}\right| + \dfrac{T_6}{T_s}\left|U_{111}\right|\cos\dfrac{\pi}{7}, \\ U_{\beta 1} = \dfrac{T_2}{T_s}\left|U_3\right|\sin\dfrac{\pi}{7} + \dfrac{T_4}{T_s}\left|U_{71}\right|\sin\dfrac{\pi}{7} + \dfrac{T_6}{T_s}\left|U_{111}\right|\sin\dfrac{\pi}{7}. \end{cases} \tag{14}$$

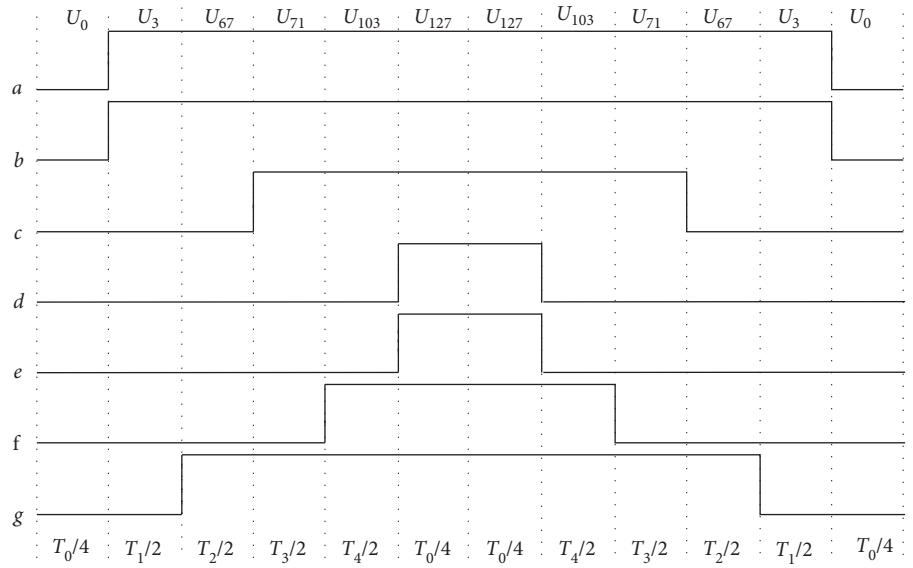

Figure 4: Switching signal of NFV-SVPWM algorithm in sector one.

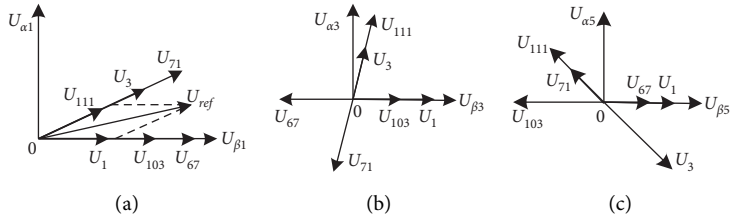

Figure 5: NSV-SVPWM vector synthesis: (a) Fundamental wave subspace. (b) The 3rd harmonic subspace. (c) The 5th harmonic subspace.

In the 3rd harmonic subspaces, the following equations are obtained:

$$\begin{cases} \dfrac{T_1}{T_s}|U_1| + \dfrac{T_5}{T_s}|U_{103}| - \dfrac{T_3}{T_s}|U_{67}| = 0, \\ \dfrac{T_2}{T_s}|U_3| + \dfrac{T_6}{T_s}|U_{111}| - \dfrac{T_4}{T_s}|U_{71}| = 0. \end{cases} \tag{15}$$

In the same way, the following equations came up in the 5th harmonic subspace

$$\begin{cases} \dfrac{T_1}{T_s}|U_1| + \dfrac{T_3}{T_s}|U_{67}| - \dfrac{T_5}{T_s}|U_{103}| = 0, \\ \dfrac{T_6}{T_s}|U_{111}| + \dfrac{T_4}{T_s}|U_{71}| - \dfrac{T_2}{T_s}|U_3| = 0. \end{cases} \tag{16}$$

According to the vector magnitude of Table 1, the substitution formulae (14)–(16), a set of equations with six variables and solving the equations can be expressed as

$$\begin{cases} T_1 = \dfrac{U_{\alpha1}\sin(\pi/7) - U_{\beta1}\cos(\pi/7)}{2.6638U_{\mathrm{dc}}\sin(\pi/7)}T_s, \\ T_2 = \dfrac{U_{\beta1}}{1.4773U_{\mathrm{dc}}\sin(\pi/7)}T_s, \\ T_3 = 2.2524T_1, \\ T_4 = 2.2524T_2, \\ T_5 = 1.8093T_1, \\ T_6 = 1.8093T_2. \end{cases} \tag{17}$$

In this way, the voltage equations are listed for each sector based on the fundamental subspace $(\alpha_1 - \beta_1)$, 3rd harmonic subspace $(\alpha_3 - \beta_3)$ and 5th harmonic subspace $(\alpha_5 - \beta_5)$, respectively. These equations are simplified to obtain a new six-element first-order functions within each sector. For example, in sector m $(1 \le m \le 14)$, the following relation holds

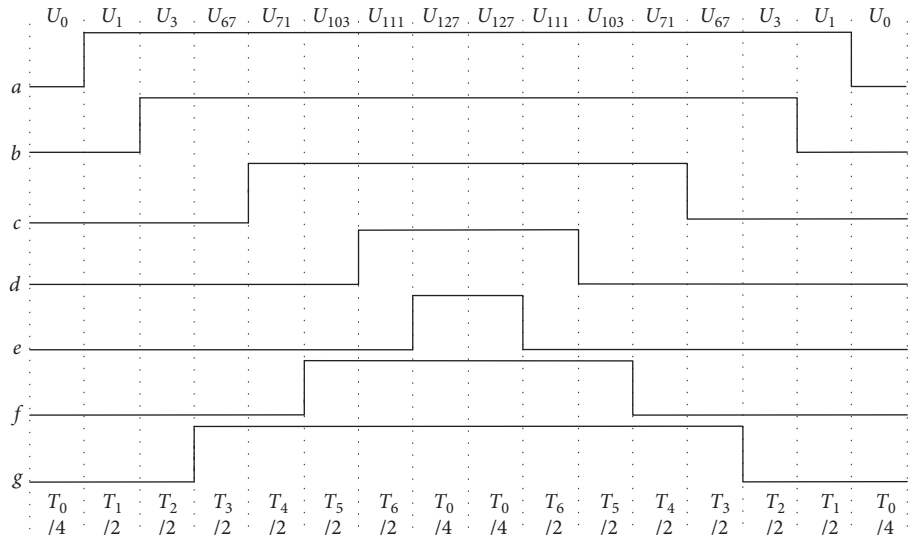

Figure 6: Switching signal of NSV-SVPWM algorithm in sector one.

$$\begin{cases} T_1 = \dfrac{U_{\beta 1}\cos[(m-1)(\pi/7)] - U_{\alpha 1}\sin[(m-1)(\pi/7)]}{1.1558U_{\mathrm{dc}}}T_s, \\ T_2 = \dfrac{U_{\alpha 1}\sin[(m-1)(\pi/7)] - U_{\beta 1}\cos[(m-1)(\pi/7)]}{0.6410U_{\mathrm{dc}}}T_s, \\ T_3 = 2.2524T_1, \\ T_4 = 2.2524T_2, \\ T_5 = 1.8093T_1, \\ T_6 = 1.8093T_2. \end{cases} \tag{18}$$

In order to reduce the switching losses, the voltage vectors for each sector should be reasonably arranged. Sector one ($m = 11$) is taken as an example for analysis. The order of action of the space voltage vector is arranged as follows: $U_0 \longrightarrow U_1 \longrightarrow U_0 \longrightarrow U_1 \longrightarrow U_3 \longrightarrow U_{67} \longrightarrow U_{71} \longrightarrow U_{103} \longrightarrow U_{111} \longrightarrow U_{71} \longrightarrow U_{67} \longrightarrow U_3 \longrightarrow U_1 \longrightarrow U_0$. The switching signal of the voltage vector in sector one is shown in Figure 6.

$$\begin{aligned} T_s &= T_1 + T_2 + T_3 + T_4 + T_5 + T_6 + T_0, \\ U_{\mathrm{ref}}T_s &= T_1U_1 + T_2U_3 + T_3U_{67} + T_4U_{71} + T_5U_{103} + T_6U_{111} + T_0. \end{aligned} \tag{19}$$

4. Simulations and Experiments Analysis

4.1. Simulations and Analysis. The proposed algorithm is implemented in Matlab/Simulink platform. The performance of the three control algorithms (NTV-SVPWM, NFV-SVPWM, and NSV-SVPWM) mentioned above section is analyzed. The parameters of the seven-phase PMSM are consistent with the mathematical model. The motor has a load of 1 N.m, the switching frequency is 20 kHz, and the DC bus voltage is 72V. The stator resistance is 1.78Ω, and d-axis inductance L_d and q-axis inductance L_q are 4.5×10^{-3} H and 4.5×10^{-3} H, respectively. The permanent magnet flux linkage ψ_f is 0.175 Wb. The moment of inertia J is $0.4 \times 10^{-3}\,\mathrm{kg \cdot m^2}$.

Simulation results of NTV-SVPWM are shown in Figure 7. In Figures 7(a) and 7(b), x-coordinate is times (s) and y-coordinate is phase current (A). It can be seen that the phase current is less sinusoidal, and the FFT harmonic analysis shows that the 3rd and 5th harmonic contents are as high as 36.65% and 17.22%, respectively, and the total harmonic THD is 40.61%. The results show that the seven-phase system extended from traditional three-phase SVPWM algorithm has the problem of harmonic phase current.

Figure 8 presents the simulation results of NFV-SVPWM. Although the sinusoidal component of the phase current is slightly higher than the NTV-SVPWM algorithm, the sinusoidal phase current is still very poor as shown in Figure 8(b). Through the FFT harmonic analysis, it can be seen that the 3rd harmonic content is much less than that of the NTV-SVPWM algorithm, only 5.31%, while the 5th harmonic content is still large, 29.13%, and the overall THD is 16.01%. Though the NFV-SVPWM algorithm controls the influence of the harmonic subspace, only the 3rd harmonic subspace is considered, and the interference of the 5th harmonic subspace is not considered, which leads to the greater content of the 5th harmonic in the phase current. In Figures 8(a) and 8(b), x-coordinate is times (s) and y-coordinate is phase current (A).

Figure 9 provides the simulation results of NSV-SVPWM. Using the same motor parameters, the simulation results show that the phase current of NSV-SVPWM appears with tiny distortion, as shown in Figure 9(b). At the same time, the phase voltage waveform is saddle waveform, as shown in Figure 9(c), where x-coordinate is times (s) and

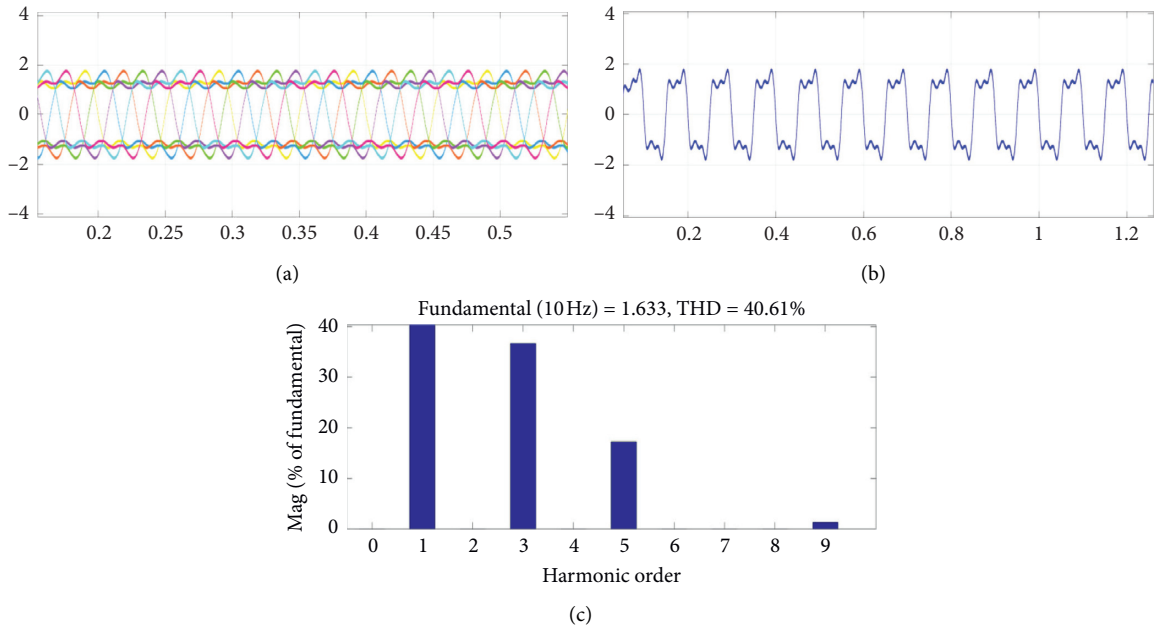

Figure 7: Simulation results of NTV-SVPWM, (a) seven-phase current waveform, (b) a phase current waveform, (c) FFT analysis.

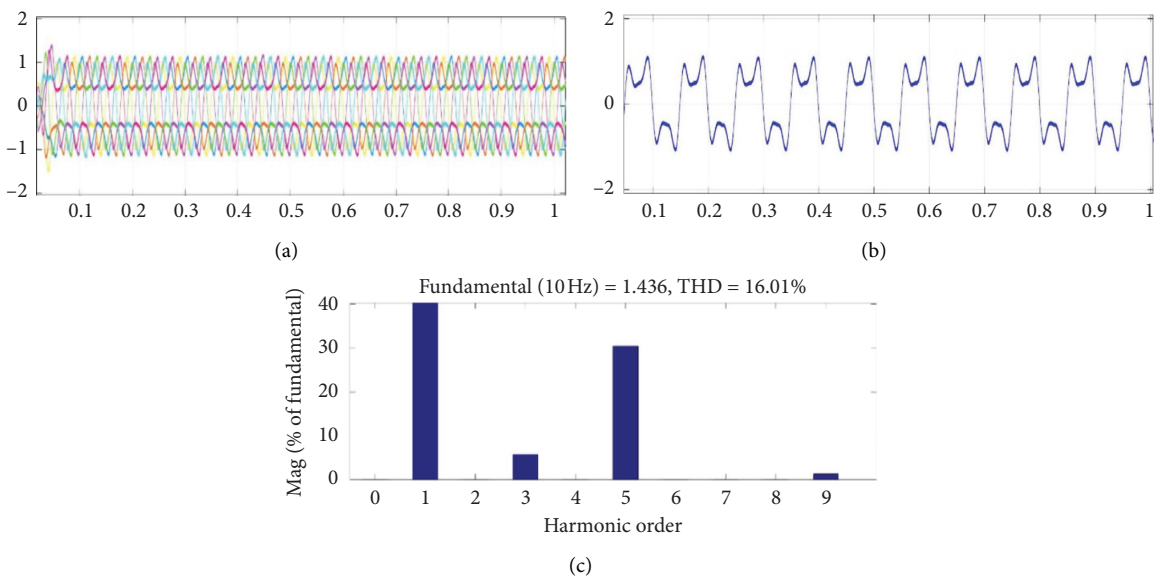

Figure 8: Simulation results of NFV-SVPWM, (a) seven-phase current waveform, (b) a phase current waveform, (c) FFT analysis.

y-coordinate is phase voltage (V). From the FFT harmonic analysis, it can be seen that the 3rd and 5th harmonic currents are much lower than those of the NTV-SVPWM algorithm, as shown in Figure 9(d). The harmonic contents of 3rd and 5th currents are only 4.29% and 1.76%, and the total THD is 3.51%.

According to the simulation results of above three algorithms, we can see that NSV-SVPWM achieves much better performance than the other methods.

4.2. Experiments and Analysis. A prototype of the proposed algorithm was then built in the lab and tested. In order to ensure that the driving system has good real-time, economic and good motor control characteristics, the STM32F407VET6 chip of the ARM Cotex-M4 kernel as the main control chip of the drive system has been used. Combined with the rated parameters of seven-phase PMSM, a motor experimental platform with a rated voltage of 72 V is built, and its physical map is shown in Figure 10.

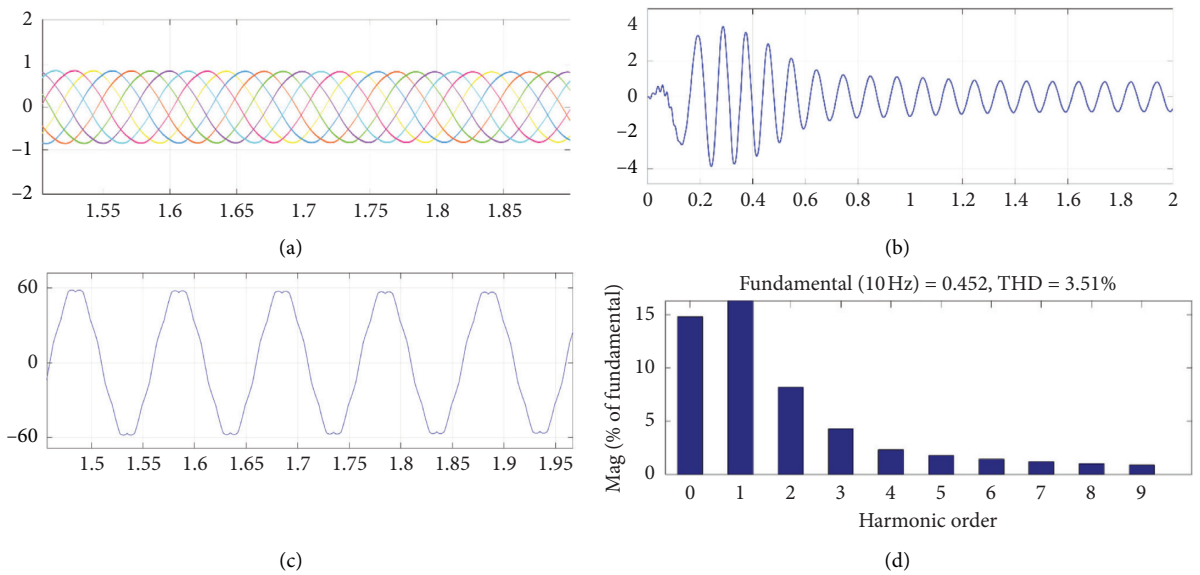

Figure 9: Simulation results of NSV-SVPWM, (a) seven-phase current waveform, (b) phase current waveform, (c) phase voltage waveform, (d) FFT analysis.

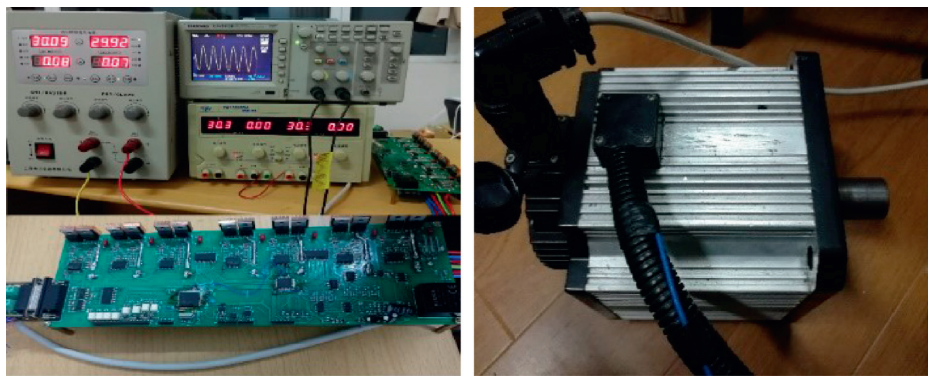

Figure 10: Seven-phase PMSM experiment platform.

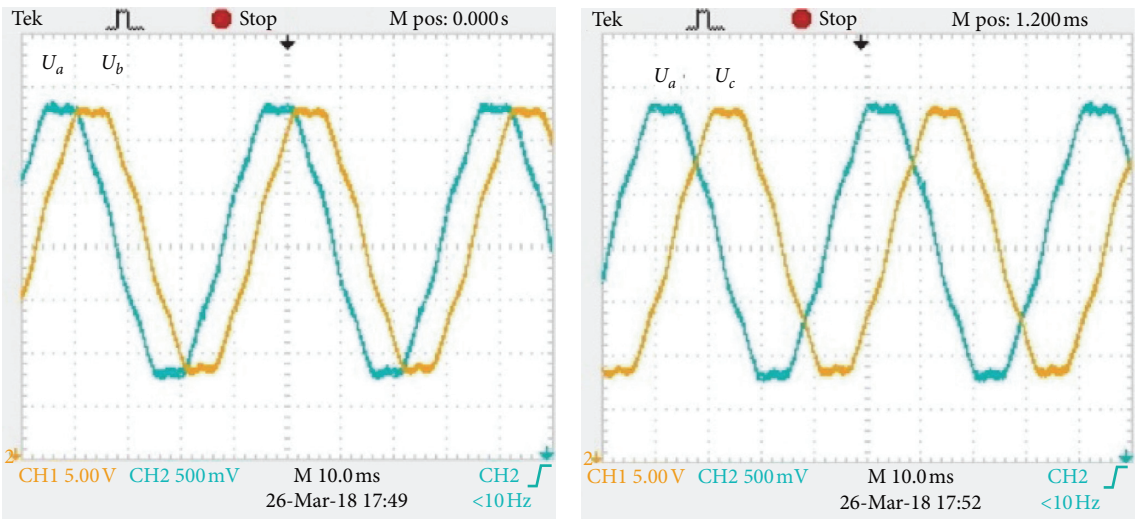

(a) (b)

Figure 11: Continued.

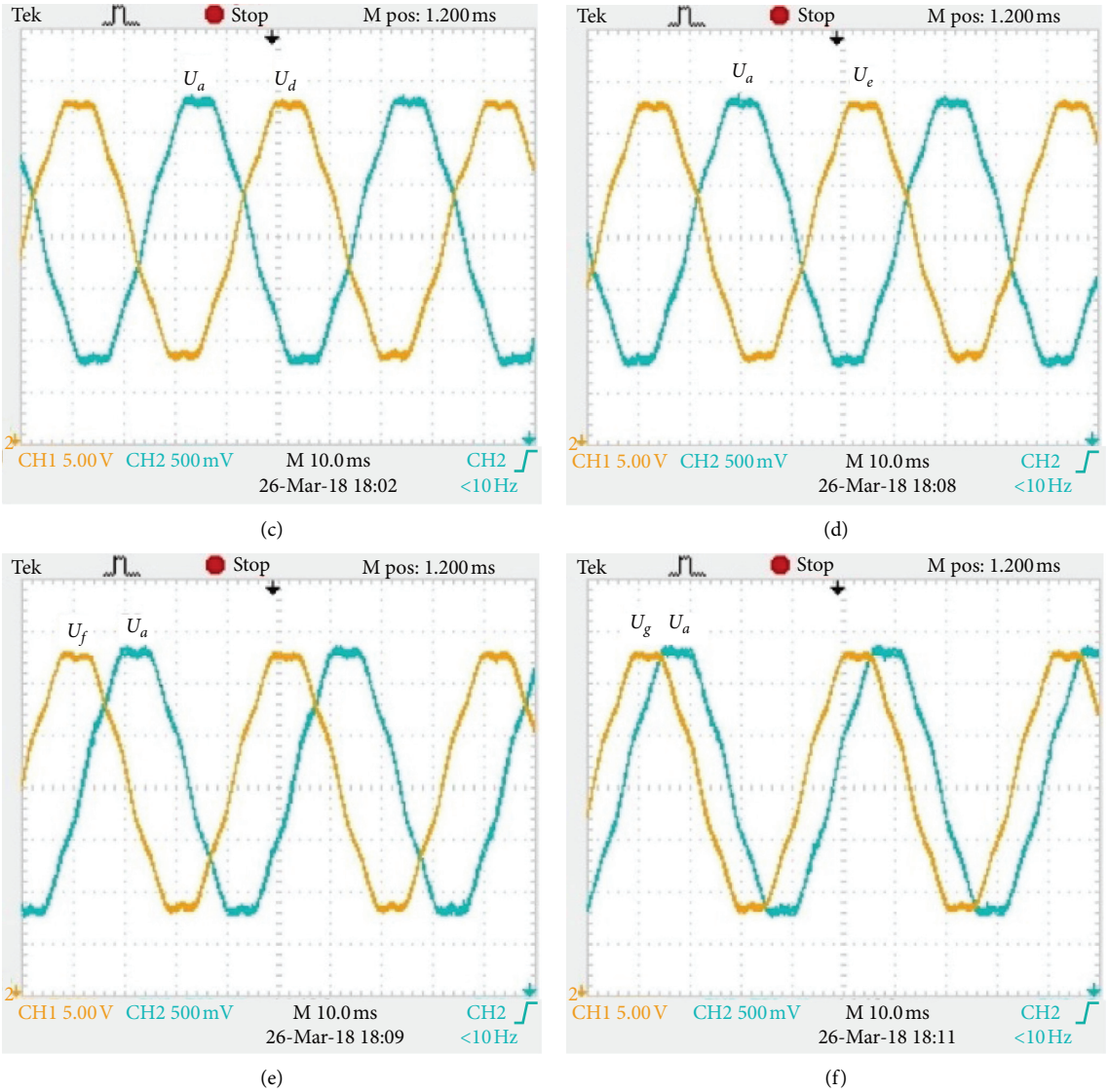

Figure 11: Phase voltage experimental waveform of NSV-SVPWM. (a) a phase and b phase voltage (b) a phase and c phase voltage, (c) a phase and d phase voltage, (d) a phase and e phase voltage, (e) a phase and f phase voltage, (f) a phase and g phase voltage.

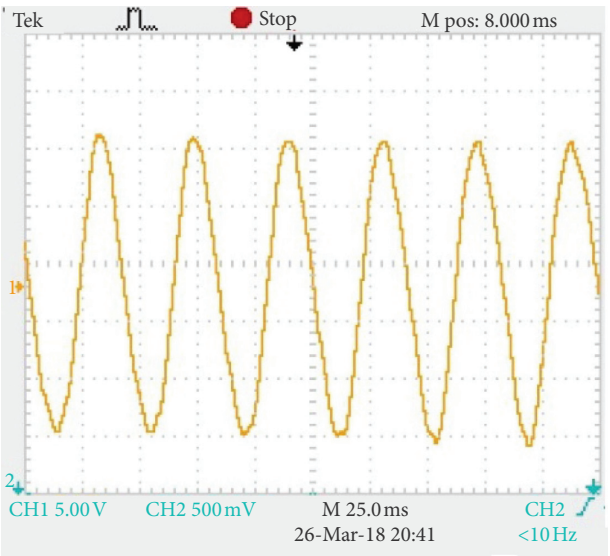

Figure 12: Phase current experimental waveform of NSV-SVPWM.

The phase voltage waveform of the NSV-SVPWM control mode is shown in Figure 11. It is not difficult to see that the phase voltage waveform is saddle wave, in which the phase difference between a phase voltage U_a and b phase voltage U_b is $2\pi/7$. The difference between a phase voltage U_a and c phase voltage U_c is $4\pi/7$, as shown in Figure 11(b). In a similar fashion, a phase voltage U_a lags g phase voltage U_g $2\pi/7$, as shown in Figure 11(f). Therefore, on the basis of the experimental results, the phase voltage waveform is consistent with the simulation results.

Figure 12 presents the phase current experimental waveform i_a. The sinusoidal component of phase current is very high and without current harmonics. It proves the feasibility of the NSV-SVPWM algorithm in the seven-phase PMSM drive control system. The experiment results are in agreement with the theoretical analysis and simulation results.

5. Conclusion

Multiphase PMSM is needed to produce the sinusoidal component in the output phase voltage, without low-order harmonics. In this paper, the rotating coordinate system of the seven-phase PMSM is obtained by matrix converter. To eliminate low-order harmonics, NTV-SVPWM algorithm, NFV-SVPWM algorithm, and NSV-SVPWM algorithm are discussed thoroughly based on simulations and experiments analysis. According to the simulation and experimental results, it can be concluded that the NSV-SVPWM algorithm not only suppresses the current high order harmonics, but also has excellent control performance.

Data Availability

No data were used to support this study.

Conflicts of Interest

The authors declare that they have no known competing financial interests or personal relationships that could have appeared to influence the work reported in this paper.

Acknowledgments

This work is supported by National Natural Science Foundation of China (Nos. 61673075 and 61876024), and Partly by the Project of Talent Peak of Six Industries (2017-DZXX-001), 333 Project of Jiangsu Province (No. BRA2019284), and The Science and Technology Development Plan Project of Chang Shu (CR0201711).

References

[1] S. Ye, "Design and performance analysis of an iterative flux sliding-mode observer for the sensorless control of PMSM drives," *ISA Transactions*, vol. 94, pp. 255–264, 2019.

[2] X. Kuang, H. Guo, J. Xu, and T. Zhou, "Research on a six-phase permanent magnet synchronous motor system at dual-redundant and fault tolerant modes in aviation application," *Chinese Journal of Aeronautics*, vol. 30, no. 4, pp. 1548–1560, 2017.

[3] A. Hosseyni, R. Trabelsi, M. F. Mimouni, A. Iqbal, and R. Alammari, "Sensorless sliding mode observer for a five-phase permanent magnet synchronous motor drive," *ISA Transactions*, vol. 58, pp. 462–473, 2015.

[4] H. Xu, S. Xue, and C. Fang, "Multiphase permanent magnet synchronous motor harmonic control base on carrier-based PWM technology," in *Proceedings of the IEEE Conference and Expo Transportation Electrification Asia-Pacific*, pp. 1–7, Beijing, China, September 2014.

[5] S. Xue, H. Xu, and C. Fang, "Multiphase permanent magnet synchronous motor harmonic plane control based on carrier technology," *Journal of Harbin Institute of Technology*, vol. 46, no. 4, pp. 122–128, 2014.

[6] L. Yuan, M. Chen, J. Shen, and F. Xiao, "Current harmonics elimination control method for six-phase PM synchronous motor drives," *ISA Transactions*, vol. 59, pp. 433–449, 2015.

[7] S. Xue and X. Wen, "Simulation analysis of a novel multiphase SVPWM strategy," in *Proceedings of the 2006 2nd International Conference on Power Electronics and Drives Systems*, pp. 756–760, Hong Kong, China, November 2006.

[8] O. Lopez, J. Alvarez, J. Malvar et al., "Space-vector PWM with common-mode voltage elimination for multiphase drives," *IEEE Transactions on Power Electronics*, vol. 31, no. 12, pp. 8151–8161, 2016.

[9] S. M. Dabour, S. M. Allam, and M. Essam, "Rashad space vector PWM technique for a novel three-to-seven phase matrix converter," in *Proceedings of the 39th Annual Conference of the IEEE Industrial Electronics Society*, pp. 4949–4954, Vienna, Austria, November 2013.

[10] O. Dordevic, E. Levi, and M. Jones, "A vector space decomposition based space vector PWM algorithm for a three-level seven-phase voltage source inverter," *IEEE Transactions on Power Electronics*, vol. 28, no. 2, pp. 637–649, 2013.

[11] F. Yu, X. Zhang, and H. Li, "The space vector PWM control research of a multiphase permanent magnet synchronous motor for electrical propulsion," *International Conference on Electrical Machines and Systems*, vol. 2, pp. 604–607, 2003.

[12] G. Grandi, G. Serra, and A. Tani, "Space vector modulation of a seven-phase voltage source inverter," in *Proceedings of the International Symposium on Power Electronics, Electrical Drives, Automation and Motion*, pp. 1149–1156, Taormina, Italy, June 2006.

[13] J. Pradeep and R. Devanathan, "Comparative analysis and simulation of PWM and SVPWM inverter fed permanent magnet synchronous motor," in *Proceedings of the International Conference on Emerging Trends in Electrical Engineering and Energy Management*, pp. 299–305, Roorkee, India, Feburary 2013.

[14] D. Casadei, D. Dujic, E. Levi, G. Serra, A. Tani, and L. Zarri, "General modulation strategy for seven-phase inverters with independent control of multiple voltage space vectors," *IEEE Transactions on Industrial Electronics*, vol. 55, no. 5, pp. 1921–1932, 2008.

[15] D. Zhang, B. Xu, H. Yang, and P. Zhu, "Simulation analysis of SVPWM based on seven-phase permanent magnet synchronous motor," in *Proceedings of the International Conference on Control, Automation and Information Sciences (ICCAIS)*, pp. 251–256, Ansan, South Korea, October 2017.

[16] W. Gong, Y. Wang, Z. Cai, and L. Wang, "Finding multiple roots of nonlinear equation systems via a repulsion-based adaptive differential evolution," *IEEE Transactions on Systems, Man, and Cybernetics: Systems*, vol. 50, no. 4, pp. 1499–1513, 2020.

[17] S. Li, W. Gong, X. Yan et al., "Parameter extraction of photovoltaic models using an improved teaching-learning-based optimization," *Energy Conversion and Management*, vol. 186, pp. 293–305, 2019.

[18] S. M. Dabour, "Space vector PWM technique to reduce common mode voltage for seven-phase inverters," in *Proceedings of the International Middle East Power Systems Conference, MEPCON*, Al Mansoura, Egypt, December 2015.

[19] S. Morimoto, Y. Takeda, K. Hatanaka et al., "Design and control system of inverter-driven permanent magnet synchronous motors for high torque operation," *IEEE Transactions on Industry Application*, vol. 29, no. 6, pp. 1150–1155, 2005.

[20] P. Zheng, P. Wang, Y. Sui, C. Tong, F. Wu, and T. Li, "Near-Five-vector SVPWM algorithm for five-phase six-leg inverters under unbalanced load conditions," *Journal of Power Electronics*, vol. 14, no. 1, pp. 61–73, 2014.